

Measurements of cosmic rays at the highest energies with the Pierre Auger Observatory

de Mello Neto, J. R. T.¹, for the Pierre Auger Collaboration²

*Instituto de Física, Universidade Federal do Rio de Janeiro, Ilha do Fundão
Rio de Janeiro, RJ Brazil*

Observatorio Pierre Auger, Av. San Martín Norte 304, 5613 Malargüe, Argentina

Abstract

This paper summarizes the status and the recent measurements from the Pierre Auger Observatory. The energy spectrum is described and its features discussed. We report searches for anisotropy of cosmic ray arrival directions on large scales and through correlation with catalogues of celestial objects. We also present the search for anisotropies in the data without the use of astronomical catalogues. The first measurement of the proton-air cross section around 10^{18} eV is discussed. Finally, the mass composition is addressed with measurements of the variation of the depth of shower maximum with energy and with the muon density at ground.

Keywords: ultra high energy cosmic rays; cosmic ray experiments

1. Introduction

Cosmic rays are energetic particles from space incident on the Earth's atmosphere, e.g. protons, heavier nuclei, photons and neutrinos, plus the secondary particles that are generated as they traverse the atmosphere. The study of cosmic ray physics had a pioneer role in the study of elementary particles and their interactions. The nature and origin of the Ultra High Energy Cosmic Rays (UHECR - here standing for cosmic rays with energy $E \geq 0.1$ EeV, $1 \text{ EeV} \equiv 10^{18}$ eV) remain puzzles almost fifty years since cosmic rays with energies of the order of 100 EeV were first reported (Linsley, 1963).

¹*E-mail address* jtmn@if.ufrj.br

²Full author list: http://www.auger.org/archive/authors_2012_07.html

The UHECRs are the subject of extensive studies including measurements of the energy spectrum, the nature of the primaries and the identification of possible sources. With energies that can reach about two orders of magnitude higher than the ones possible in the LHC, the study of the UHECRs probes the hadronic interactions in otherwise inaccessible regions of the phase space.

2. The Pierre Auger Observatory

The Pierre Auger Observatory ([Abraham et al., 2004](#)) is the world’s largest UHECR facility, conceived to measure the flux, arrival direction distribution and mass composition of cosmic rays from 0.1 EeV (low energy extensions included ([Hermann-Josef Mathes, 2011](#)) ([Wundheiler, 2011](#))) to the highest energies with high statistical significance. It is a hybrid detector that combines both surface and fluorescence detectors at the same site. The surface detector (SD) consists of 1660 $10\text{m}^2 \times 1.2\text{m}$ water-cherenkov stations deployed over 3000 km^2 on a 1500 m triangular grid. An “infill” array with a 750 m grid was added to the SD with the purpose of measuring showers of lower energy. The SD is overlooked by a fluorescence detector (FD) composed of four fluorescence stations, each one with 6 wide angle telescopes, and one additional station with 3 high-elevation telescopes also conceived to measure showers of lower energy. The surface detector stations sample the electrons, photons and muons in the shower front at ground level. The fluorescence telescopes can record ultraviolet light emitted as the shower crosses the atmosphere, allowing one to observe the longitudinal development of the air shower. The fluorescence detector operates only on clear, moonless nights, so its duty cycle is about 13%. On the other hand, the surface detector array has a duty cycle close to 100%.

3. The cosmic ray energy spectrum

It is crucial to measure accurately the cosmic ray flux above 10^{18} eV in order to discriminate among different models describing the transition between galactic and extragalactic cosmic rays and between the suppression induced by the cosmic ray propagation and features of the injection spectrum of the sources. The energy spectrum was measured by the Pierre Auger Observatory and here we report the combined measurements ([Abraham et al., 2010a](#)), ([Salamida, 2011](#)) of the SD and the hybrid data. The SD-only events used in [Fig. 1](#) were taken between 1 January 2004 and 31 December 2010, with a

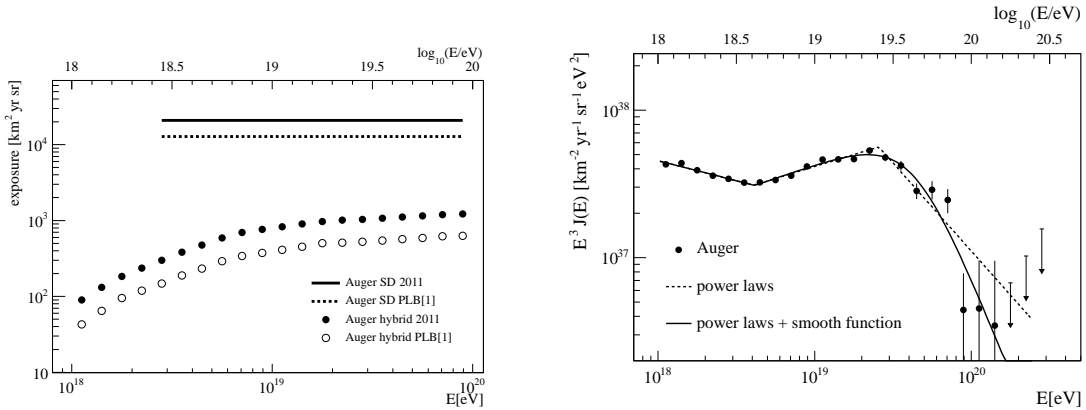


Figure 1: Left: The SD and hybrid exposures used for the current flux measurement compared with a previously published data set (Abraham et al., 2010a). The SD exposure is shown for energies higher than $10^{18.5}$ eV where the detector is fully efficient. Right: The combined energy spectrum is fitted with two functions. Only statistical uncertainties are shown. The systematic uncertainty in the energy scale is 22%.

total exposure of 20905 km² sr yr, while the hybrid events were recorded from 1 November 2005 to 30 September 2010. The higher energies are more easily accessible to the SD that has larger exposure. The points at the low end of the plotted spectrum are obtained from the Auger hybrid events. The hybrid events are defined by the simultaneous triggering of a fluorescence telescope and at least one surface detector station. The lower energy threshold and good energy resolution of those events enable measurements to be extended to 10^{18} EeV. The exposure of the hybrid mode of the Pierre Auger Observatory has been calculated using a time-dependent Monte Carlo simulation. The changing configurations of both fluorescence and surface detectors are taken into account for the determination of the on-time of the hybrid system, see Fig. 1 (left plot). The two spectra were combined using a maximum likelihood method. They have the same systematic uncertainty in the energy scale (22%), but the normalization uncertainties are independent, 6% for the SD data and between 6% and 10% for the hybrid data. In the region where both distributions overlap (from about 3×10^{18} eV to about 7×10^{19} eV) they are mutually consistent within the normalization uncertainties.

A piecewise fit using power laws ($dN/dE \sim E^{-\alpha}$) and another one using power laws plus a smooth function are shown in the plot of Fig. 1 (right plot). We can see that there are two clear spectral features: at 4.1 EeV ($10^{18.61}$ eV) and 26 EeV ($10^{19.41}$ eV). The first feature is known as the

ankle, where the spectral index changes from $\alpha = 3.27 \pm 0.02$ to 2.68 ± 0.01 . The spectrum is steeper after the second feature (the power law fit taking the value $\alpha = 4.2 \pm 0.1$) and is compatible with the "GZK suppression", predicted by Greisen, Zatsepin and Kuz'min (Greisen, 1966), (Zatsepin and Kuzmin, 1966) immediately after the discovery of the cosmic microwave background (CMB). As shown in Fig. 1 (right plot) the combination of the two spectra has enabled the precise measurement of the ankle and of the flux suppression at high energies.

The physical origin of the ankle is not settled yet. There are two main candidate scenarios to explain it. In the first scenario the models relate the ankle to the transition from a galactic component to a harder extragalactic one (Linsley, 1967), (Hillas, 1967). The second scenario involves models in which cosmic rays are supposed to be extragalactic protons down to energies below 1 EeV and the concave shape is due to the effect of energy losses of the protons by pair creation with CMB photons, the so-called dip scenario (Berezinsky, Gazizov and Grigorieva, 2005). In order to elucidate this issue, anisotropy measurements are very important (and will be discussed in the following session). Measurements of composition are also important because one expects that heavy nuclei dominate galactic cosmic rays at EeV energies, since their confinement by galactic magnetic fields is a rigidity dependent effect.

The suppression at the highest energies, measured with unprecedented statistical significance, is consistent with the expectations from the so called "GZK suppression", understood as the attenuation of extragalactic protons by photo-pion production off CMB photons or as the suppression of nuclei by photodesintegration. However, it must be noted that the interpretation of the flux suppression in terms of interactions with the CMB does not exclude additional contributions related to the acceleration mechanism, such as a change in the injection spectrum at the source or the maximum energy of the accelerators.

4. Studies of anisotropy in the arrival direction of the UHECRs

As mentioned in the previous section, if the ankle is due to the change from a galactic to an extragalactic component, a dipolar modulation in the cosmic ray arrival directions is expected. The amplitude of the dipole should increase with energy up to the ankle, reaching a level of a few percent, even if primaries are heavy nuclei. Predictions of the amplitude and orientation

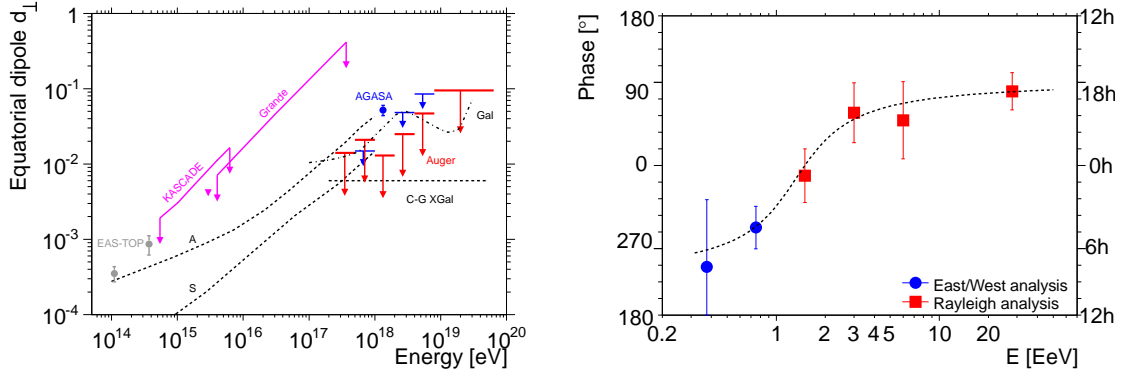


Figure 2: Left: Upper limits on the anisotropy of first harmonic amplitude as a function of energy and model predictions (see text). Right: Phase of the first harmonic as a function of energy. The dotted line represents a hypothetical smooth transition of the dipole direction.

of the dipole depend on the magnitude of the magnetic field and also on the source distribution. If the dip scenario is the correct explanation for the ankle, it means that UHECRs above 10^{18} eV are already dominated by the extragalactic component, and their flux is expected to be highly isotropic. However a dipole of less than one percent amplitude is still expected due to the *Compton-Getting effect*. It would produce a dipolar distribution constant with energy and with an orientation related to the relative movement of the Earth with respect to the "rest frame" of the extragalactic cosmic rays.

The distribution in right ascension of the flux of CRs arriving at a detector can be characterized by the amplitudes and phases of its Fourier expansion. Our aim is to determine the first harmonic amplitude r and its phase ϕ . The phase indicates the direction of the dipole in right ascension.

Thanks to the high statistics of the SD data a first harmonic analysis was performed in different energy ranges starting from 2.5×10^{17} eV in search for dipolar modulations in right ascension (Abraham et al., 2011), (Lyberis, 2011). This analysis used the fact that the exposure is almost uniform in right ascension.

Below $E \sim 1$ EeV, the detection efficiency of the array depends on zenith angle and composition, which amplifies detector-dependent variations in the counting rate. Consequently, our results below 1 EeV are derived using simple event counting rate differences between Eastward and Westward directions. That technique using relative rates allows a search for anisotropy in

right ascension without requiring any evaluation of the detection efficiency. The angular resolution is defined as the angular aperture around the arrival directions of cosmic rays within which 68% of the showers are reconstructed. At the lowest observed energies, events trigger as few as three surface detectors. The angular resolution of events having such a low multiplicity is contained within 2.2° , which is quite sufficient to perform searches for large-scale patterns in arrival directions, and reaches $\sim 1^\circ$ for events with multiplicities larger than five.

No significant amplitude was detected. The 99% CL upper limits as a function of energy are shown in Fig. 2 (left plot) together with predictions from two different galactic magnetic field models (A and S), for a purely galactic origin of UHECRs (Gal), and the expectations from the Compton-Getting effect (C-G Xgal) (Abraham et al., 2011). A particular model with an antisymmetric halo magnetic field (A) is already excluded by the upper limits. In Fig. 2 (right plot) the phase measurement as a function of the energy shows an interesting pattern: it suggests a smooth transition between a phase of $\sim 270^\circ$ (consistent with the right ascension of the galactic center) below 1×10^{18} eV and another phase of $\sim 90^\circ$ (consistent with the right ascension of the galactic anti-center) above 5×10^{18} eV. This is interesting since a real anisotropy would need less events to be established with high statistical confidence through phase consistency in ordered energy intervals rather than by amplitude measurements (Abraham et al., 2011). New data will show if this feature still stands.

For energies up to 10^{15} eV, cosmic rays are believed to have a galactic origin and shock acceleration in supernova remnants could be the most likely source. At the highest energies, the most probable sources of ultra-high energy cosmic rays (UHECRs) are extragalactic: jets of active galactic nuclei (AGN), galaxy radio lobes, gamma ray bursts and colliding galaxies, among others (Kotera and Olinto, 2011).

The Pierre Auger Collaboration reported (Abraham et al., 2008), (Abraham et al., 2007) a correlation of its highest energy events with the AGNs in the Véron-Cetty and Véron catalogue. The first 14 events were used for an exploratory scan that yielded the following search parameters: energy threshold ($E_{th} = 55$ EeV), maximum angular separation ($\Psi \leq 3.1^\circ$) and maximum redshift ($z \leq 0.018$). Those parameters minimize the probability that the correlation with AGN could result from a background fluctuation if the flux were isotropic. The subsequent 13 events established a 99% confidence level for rejecting the hypothesis of isotropic cosmic ray flux. The reported frac-

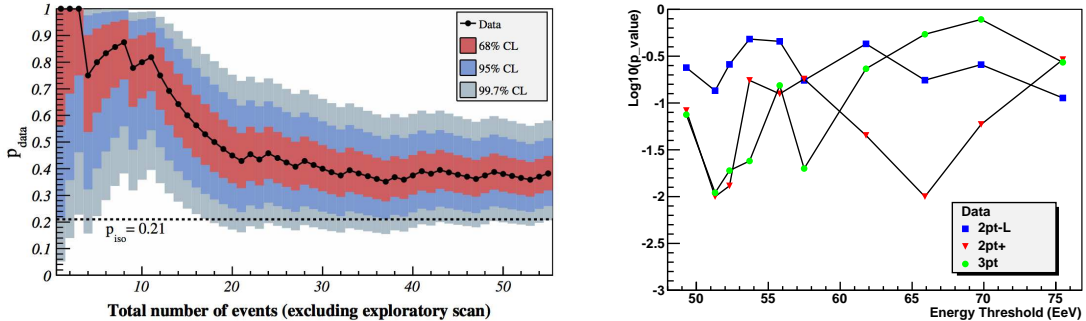


Figure 3: Left: Fraction of events correlating with AGNs as a function of the cumulative number of events, starting after the exploratory data. The expected correlating fraction for isotropic cosmic rays is shown by the dotted line. Right: The minimum in P_{value} is at 100 events for the 2pt+ and 3pt methods and corresponds to an energy of about $51 \approx \text{EeV}$.

tion of correlation events was $(69^{+11}_{-13})\%$. By adding data with $E_{th} = 55 \text{ EeV}$ up to the end of 2009 (69 events in total), the correlation level decreased to $(38^{+7}_{-6})\%$ (Abraham et al., 2010b). For this dataset, we show in Fig. 3 (left plot) the most likely value of the fraction of the correlated events, plotted with black dots as a function of the total number of time-ordered events (the events used in the exploratory scan are excluded). The most recent estimate of the fraction of correlating cosmic rays is $(33 \pm 5)\%$, with 21% expected under the isotropic hypothesis (Kampert, 2011).

A posteriori studies (Abraham et al., 2010b) showed that the distribution of arrival directions of the 69 highest energy cosmic rays is compatible with models (for suitable values of two parameters, the smoothing factor σ and an isotropic fraction f_{iso}) based on populations of nearby extragalactic objects, such as galaxies in the 2MRS and AGNs in the SWIFT-BAT catalogues. The models fit the data for smoothing angles around a few degrees and for correlating fractions of order 40% ($f_{\text{iso}} \approx 0.6$). The data do not fit either the isotropic expectation or the predictions of the models with $f_{\text{iso}} = 0$. A large isotropic fraction could indicate that the model is not using a catalogue that includes all the contributing UHECR sources or that a fraction of arrival directions are isotropized by large magnetic deflections of a highly charged particle component.

The UHECR anisotropy can also be studied with the use of catalog independent methods. In (Abreu et al., 2012a) three methods, named 2pt-L, 3pt

and 2pt+, each giving a different measure of self-clustering in arrival directions, were tested on mock data sets. The impact of sample size and magnetic smearing was studied. These studies suggested that the three methods could efficiently respond to a real anisotropy in the data with a $P_{\text{value}} = 1\%$ or smaller with a data set of the order of one hundred events. The methods were applied to the data from the 20 highest energy events to the highest 110. As shown in Fig. 3 (right plot), the two most powerful methods (3pt and 2pt+) show a minimum in the distribution of P_{value} as a function of the energy threshold for an energy around 51 EeV, (i.e., at 100 events) (Abreu et al., 2012a). But there is no P_{value} smaller than 1% in any of the 30 (correlated) scanned values. There is thus no strong evidence of clustering in the data set which was examined. In case there is a true weak anisotropy in the data, the common minimum could indicate the onset of this anisotropy, while the less powerful method (2pt-L) would not have detected it. For higher energy thresholds the number of events decreases and the power of the methods diminish as expected. Simulations show (Abreu et al., 2012a) that this null result is compatible with the correlation with the VCV catalogue discussed above.

5. Mass composition

The measurement of the mass composition of UHECRs is essential to the solution of the problem of their origin, since the mass, and charge Z , distribution can give powerful constraints on their acceleration mechanisms and propagation. For UHECRs the main observable sensitive to composition is the $\langle X_{\text{max}} \rangle$, the average value of the atmospheric depth (measured in g/cm^2) where the shower development reaches its maximum. Proton showers are about $100 \text{ g}/\text{cm}^2$ deeper in the atmosphere than iron showers. In a similar way, the fluctuation of the values of X_{max} around the mean depth, $\text{RMS}(X_{\text{max}})$, provides another sensitive observable: iron showers fluctuate about $40 \text{ g}/\text{cm}^2$ less than proton showers. Those estimates are obtained from transport codes that simulate shower development given a model for hadronic interactions. The energy evolution of the two mentioned observables for proton and iron and several hadronic models are shown in Fig. 4 together with the FD data (Facal San Luis, 2011), (Abreu et al., 2010). Both plots could be interpreted as an evolution from light to heavier composition if current hadronic interaction models adequately describe the air shower physics.

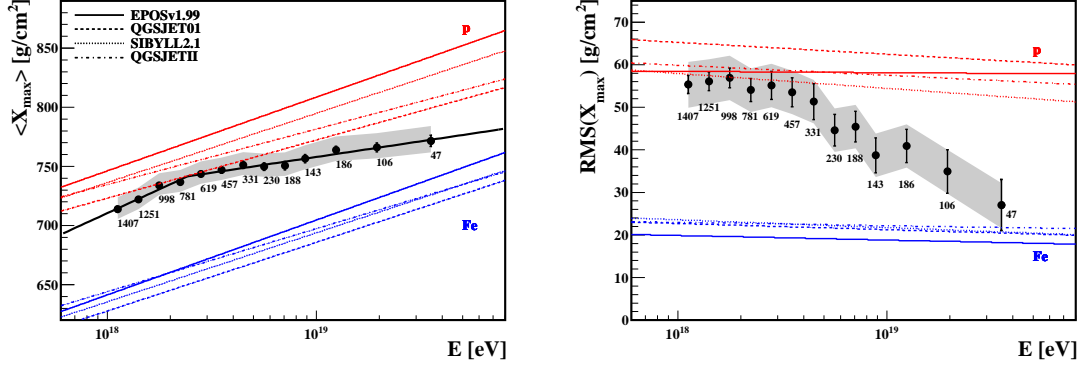


Figure 4: Left: $\langle X_{\max} \rangle$ as a function of energy. Right: $\text{RMS}(X_{\max})$ as a function of the energy. In both plots data (points) are shown with the predictions for proton and iron for several hadronic interaction models. The number of events in each bin is indicated. Systematic uncertainties are indicated as a band.

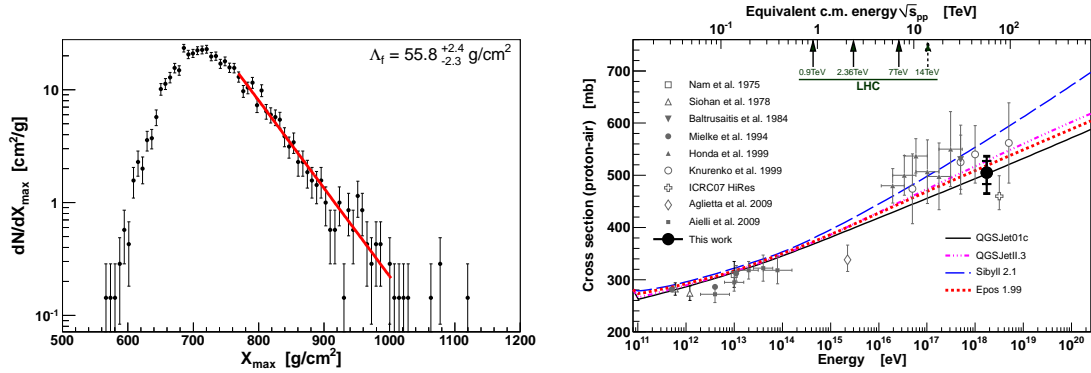


Figure 5: Left: Unbinned likelihood fit of the tail of the X_{\max} distribution. Right: Resulting σ_{p-air} compared to other measurements and model predictions. The inner error bars are statistical only, while the outer include all systematic uncertainties for a helium fraction of 25% and 10 mb photon systematics.

An analysis of the proton-air cross-section based on the shape of the distribution of X_{\max} was presented in (Abreu et al., 2012b). That analysis is based on the fact that the tail of the X_{max} distribution is sensitive to σ_{p-air} . The longitudinal profile of the energy deposit is reconstructed from the light recorded by the Fluorescence detector. With the help of data from atmospheric monitoring devices the light collected by the telescopes is corrected for the attenuation between the shower and the detector and the longitudinal shower profile is reconstructed as a function of atmospheric depth. X_{\max} is determined by fitting the reconstructed longitudinal profile with a Gaisser-Hillas function (Gaisser and Hillas, 1977). The typical resolution is around 20 g/cm² above a few EeV. In fact, the cross section is directly related to the exponential distribution of the depth of the first interaction X_1 which is not accessed experimentally. The strong correlation between X_1 and X_{\max} makes the distribution of the latter sensitive to the proton-air cross-section and the tail of the distribution maximizes the proton content, since it is the most penetrating nucleus. A slope obtained from a fit to the exponential tail of the X_{max} distribution (see left of Fig 5) can be used as an estimator for σ_{p-air} through Monte Carlo simulations: the cross-section is rescaled consistently to reproduce the value of the measurement. The lack of detailed knowledge of the mass composition at these energies turns out to be the main difficulty for this analysis, since one cannot exclude contamination by photons and helium primaries, for instance. This translates into the main contribution to the systematic uncertainty of this measurement. Only events with energy between 10¹⁸ eV and 10^{18.5} eV were used and the average center-of-mass energy is $\sqrt{s} = 57$ TeV. If the possible presence of helium in the data sample is neglected, the measured proton-air cross-section is $\sigma_{p-air} = 505 \pm 22(\text{stat})_{-36}^{+28}(\text{sys})$ mb.

Another estimator of the composition of the primary particles is the muon density on ground. The muon density on the ground is predicted to be 30-40% larger for iron primaries than for proton primaries. The value of this ratio is considered robust, as opposed to the absolute value of the muon density that is more model dependent.

The fraction of the signals in the SD from the muonic component and from the electromagnetic component of the shower is measured in two ways. The most direct one to investigate the muon content of the cosmic ray showers is through the study of very inclined events (Dembinsky, 2011). In those events the dominant particles at ground are muons since the electrons and photons were absorbed by the atmosphere. The observable N_{19} is the muon

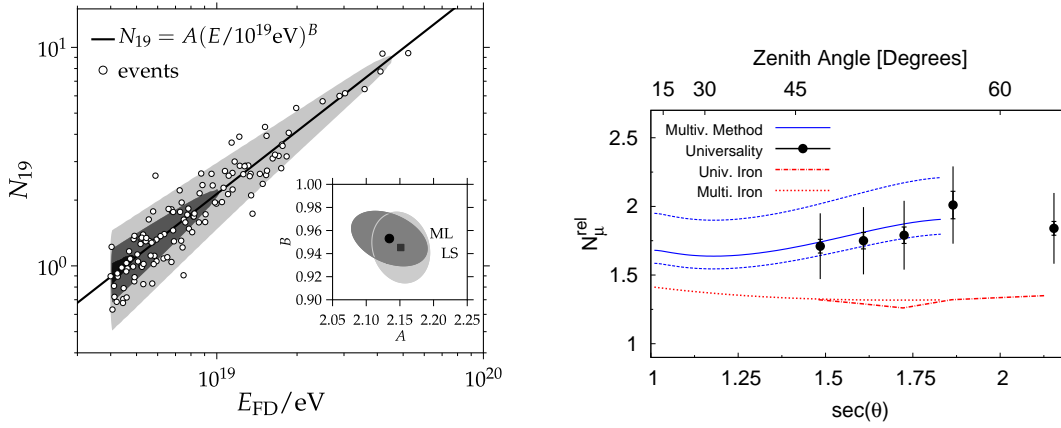


Figure 6: Left: Fit of the calibration curve $N_{19} = A(E_{FD}/10^{19}\text{eV})^B$ to 125 events. The contours indicate constant levels of the p.d.f. that models the observed $(E_{FD}, N_{19}$ and θ) integrated over θ , corresponding to 10, 50, 90% of the maximum value. The calibration constants A, B obtained with the maximum-likelihood method (ML) and a least-squares method (LS) are shown in the inset. The ellipses indicate uncertainty contours of 68% confidence. Right: The number of muons estimated at 1000 m in data relative to the predictions of simulations using QGSJET II with proton primaries. The results obtained using multivariate method are shown as the solid line with systematic uncertainties as the dashed lines. The results obtained using the universality of S_μ/S_{em} are shown as circles with statistical and systematic uncertainties. The results when the methods are applied on a library of iron-initiated showers are shown as the dot and dash-dot lines at 10^{19} eV.

estimator that in fact is the measured shower size. For inclined showers, the energy of the primary is obtained by calibrating N_{19} with the calorimetric energy E_{FD} from high-quality events measured simultaneously with the fluorescence detector and the surface detector for inclined showers. The plot on the left of Fig. 6 shows the correlation between N_{19} and E_{FD} . N_{19} is parameterized (Dembinsky, 2011) as a function of E_{FD} with the fitting function $N_{19} = A(E_{FD}/10^{19}\text{eV})^B$. For this particular choice, A is the relative number of muons with respect to the reference distribution at 10 EeV. The slope $d \ln(N_{19})/d \ln(E_{FD})$ of the relative number of muons is given by parameter B , and carries information about possible changes in $\langle \ln(A) \rangle$.

Using usual (not very inclined) events one can compare data from the SD and FD simultaneously, on a event-by-event basis, to the result of simulations, or use the time structure of the signals in the surface detectors and an universal property of air showers to estimate the number of muons in the data (Allen, 2011). A summary of the results obtained with these two methods when applied to data is shown in the right of Fig. 6. Simulations of air showers using QGSJET II with proton and iron primaries underestimate both the total detector signal at ground level and the number of muons in events collected at the Pierre Auger Observatory. These discrepancies could be caused by an incorrect energy assignment within the 22% systematic uncertainty of the energy scale of the Auger Observatory and/or shortcomings in the simulation of the hadronic and muonic shower components. All results point to the fact that simulations of proton primaries and iron primaries underestimate the muon fraction at ground level.

6. Conclusions

The Pierre Auger Observatory has detected high quality events and has made key measurements of the highest-energy cosmic rays. In spite of that, many issues remain open. The spectrum suppression is well established but it is not known if this is due to the GZK effect or if it is due to the maximum energy attained in astrophysical accelerators. Measurements of the large scale anisotropy provides upper limits in the dipole amplitude that constrain theoretical models in the ankle region. The Pierre Auger Observatory data provide evidence for a correlation between arrival directions of cosmic rays above 55 EeV and the positions of AGNs with $z < 0.018$. The estimated fraction of correlating cosmic rays is currently about 33% compared with 21% expected for isotropy.

The first measurement of the cross section proton-air around 10^{18} eV was presented. Detailed studies of hadronic interactions in the atmosphere together with a much larger sample may provide new information that will help to answer the questions raised by the UHECRs.

7. References

References

- Abraham, J., Aglietta, M., Aguirre, I.C. et al. [The Pierre Auger Collaboration], Properties and performance of the prototype instrument for the Pierre Auger Observatory, Nucl. Instr. and Meth. in Phys. Res. A 523, 50-95, 2004.
- Abraham, J., Abreu, P., Aglietta, M. et al. [The Pierre Auger Collaboration], Correlation of the Highest-Energy Cosmic Rays with Nearby Extragalactic Objects, Science, 318, 938-943, 2007.
- Abraham, J., Abreu, P., Aglietta, M. et al. [The Pierre Auger Collaboration], Correlation of the highest-energy cosmic rays with the positions of nearby active galactic nuclei, Astropart. Phys. 29, 188-204, 2008.
- Abraham, J., Abreu, P., Aglietta, M. et al. [The Pierre Auger Collaboration], Measurement of the energy spectrum of cosmic rays above 10^{18} eV using the Pierre Auger Observatory, Phys. Lett. B 685, 239-246, 2010.
- Abraham, J., Abreu, P., Aglietta, M. et al. [The Pierre Auger Collaboration], Update on the correlation of the highest energy cosmic rays with nearby extragalactic matter, Astropart. Phys. 34, 314-326, 2010.
- Abreu, P., Aglietta, M., Ahn, E.J., et al. [The Pierre Auger Collaboration], Search for First Harmonic Modulation in the Right Ascension Distribution of Cosmic Rays Detected at the Pierre Auger Observatory, Astropart. Phys. 34, 627-639, 2011.
- Abreu, P., Aglietta, M., Ahn, E.J. et al., [The Pierre Auger Collaboration], Measurement of the Depth of Maximum of Extensive Air Showers above 10^{18} eV, Phys. Rev. Lett. 104, 091101, 2010.

- Abreu, P., Aglietta, M., Ahlers, M. et al. [The Pierre Auger Collaboration], A search for anisotropy in the arrival directions of ultra high energy cosmic rays recorded at the Pierre Auger, *J. Cosmol. Astropart. Phys.* JCAP04(2012)040, 2012.
- Abreu, P., Aglietta, M., Ahlers, M. et al., [The Pierre Auger Collaboration], Measurement of the proton-air cross-section at $\sqrt{s} = 57$ TeV with the Pierre Auger Observatory, *Phys. Rev. Lett.* 109, 062002, 2012.
- Allen, J. [The Pierre Auger Collaboration], Interpretation of the signals produced by showers from cosmic rays of 10^{19} eV observed in the surface detectors of the Pierre Auger Observatory, Proc. 32nd ICRC, Beijing, China, Preprint 1107.4804v1, 2011.
- Berezinsky, V., Gazizov, A. Z. and Grigorieva, S. I., Dip in UHECR spectrum as signature of proton interaction with CMB, *Phys.Lett.* B612, 147-153, 2005.
- Dembinsky, H. P. [The Pierre Auger Collaboration], The cosmic ray spectrum above 4×10^{18} eV as measured with inclined showers recorded at the Pierre Auger Observatory, Proc. 32nd ICRC, Beijing, China, Preprint 1107.4809v1, 2011.
- Facal San Luis, P. [The Pierre Auger Collaboration], The distribution of shower maxima of UHECR air showers, Proc. 32nd ICRC, Beijing, China, Preprint 1107.4804v1, 2011.
- Gaisser, T. K. and Hillas, A. M., Reliability of the method of constant intensity cuts for reconstructing the average development of vertical showers, Proc. 15th ICRC, Plovdiv, Bulgaria, Vol. 8, 353-357, 1977.
- Greisen, K., End to the cosmic ray spectrum?, *Phys. Rev. Lett.* 16, 748-750, 1966.
- Hermann-Josef Mathes, T., [The Pierre Auger Collaboration], The HEAT Telescopes of the Pierre Auger Observatory Status and First Data Proc. 32nd ICRC, Beijing, China, Preprint 1107.4807, 2011
- Hillas, A. M., The energy spectrum of cosmic rays in an evolving universe, *Phys. Lett A*, 24, 677-678, 1967.

- Kampert, K-H. [The Pierre Auger Collaboration], Highlights from the Pierre Auger Observatory, Proc. 32nd ICRC, Preprint 1207.4823, 2011.
- Kotera, K. and Olinto A. V., The Astrophysics of Ultrahigh Energy Cosmic Rays, Annu. Rev. Astron. Astrophys. **49** 119-153, 2011.
- Linsley, J., Evidence for a primary cosmic-ray particle with energy 10^{20} eV, Phys. Rev. Lett. 10, 146-148, 1963.
- Linsley, J., Air shower fluctuations, Proc. of 8th ICRC, Jaipur, India, 4, 77-99, 1963.
- Lyberis, H. [The Pierre Auger Collaboration], Analysis of the modulation in the first harmonic of the right ascension distribution of cosmic rays detected at the Pierre Auger Observatory, Proc. 32nd ICRC, Beijing, China, Preprint 1107.4805, 2011.
- Salamida, F [The Pierre Auger Collaboration], Update on the measurement of the CR energy spectrum above 10^{18} eV made using the Pierre Auger Observatory, Proc. 32nd ICRC, Beijing, China, Preprint 1107.4809v1, 2011.
- Wundheiler B [The Pierre Auger Collaboration], The AMIGA muon counters of the Pierre Auger Observatory: performance and first data, Proc. 32nd ICRC, Beijing, China, Preprint 1107.4807, 2011.
- Zatsepin G. T., Kuzmin V.A., Upper limit of the spectrum of cosmic rays, Pisma Zh.Eksp. Teor. Fiz 4, 114-117, 1966.